Driven, dissipative superfluids: Radial counterflow of rotating ^{4}He

Laurence J. Campbell
Theoretical Division, Los Alamos National Laboratory, Los Alamos, New Mexico 87545
(Received 11 May 1987)

Predicting the behavior of simple two-dimensional, laminar, steady-state flow in the presence of superfluid vorticity requires extension of the two-fluid model by an additional equation for the total superfluid vorticity and by the vortex nucleation rates at the boundary. For the case of superfluid ^{4}He in a rotating annulus driven by radial counterflow, predictions are made for the dissipation, meniscus profile, heat torque, angular momentum, and positive and negative vortex densities. The sensitivity of the results to vortex nucleation rates, which are currently unknown, invites their experimental measurement.

I. INTRODUCTION

Whether in a simple bucket[1] or in the annular space between two concentric cylinders,[2] rotating superfluid helium achieves an equilibrium state consisting of an array of quantized vortices that for sufficiently fast rotation becomes uniform and causes the superfluid meniscus to equal that of a normal fluid over distances larger than the intervortex spacing. This result can be found in a number of ways from the phenomenological two-fluid equations when these are extended to include either discrete or continuous superfluid vorticity.[3] However, if a small temperature difference is imposed between the two boundaries of a rotating annulus the phenomenological two-fluid equations become inadequate to describe the resulting steady-state flow pattern, even in the simplifying case of high vortex densities where individual vortex effects are negligible. Further extension is required in the form of an equation for the *total* superfluid vortex density N; only the *net* vortex density n is determined by the curl of $\mathbf{V}_s$. It turns out that radial counterflow in a rotating annulus has no steady-state solution for which the radial inflow velocities for all vortices are zero at both inner and outer boundaries. This is also true for a nonrotating annulus, but only the case of rotation is considered here because the resulting alignment of the vortices parallel to the rotation axis is expected to justify two-dimensional calculations, especially for long, narrow cylinders.

Also needed are vortex boundary conditions that are currently unknown; namely, the nucleation rate of vortices at a boundary when hydrodynamic forces favor their entrance into the liquid. The calculations here are done for various boundary conditions that should span the effective, true value and permit an experimental estimation. Vortex line stretching that can lead to superfluid turbulence[4] is assumed to be unimportant here principally because of low counterflow velocities and the expected rectinlinear bias to the lines due to rotation.

In Sec. II driven dissipative superflow is shown to have exact solutions for restricted vortex nucleation. Numerical solutions are exhibited for unrestricted nucleation. Some predicted properties of these solutions are compared in Sec. III; namely, the dissipation, meniscus profile, heat torque, and angular momentum. Section IV contains a brief summary.

Vortex boundary conditions also affect the transient spin-up behavior of superfluid in a simple cylinder following a torque impulse. However, in this case the experimental data appear less sensitive to the details of vortex nucleation than to something else, which was interpreted as an additional drag between the vortices and container walls.[5,6] A motivation for the present work was to study vortex density variations and nucleation effects in a context that allows (hopefully) easier experimental control, i.e., involving steady-state instead of transient processes.

II. EQUATIONS AND SOLUTIONS

A. Basic equations

All equations apply to the laboratory frame, with the axis of rotation and the rectinlinear vortices parallel to the $\hat{\mathbf{z}}$ axis. The macroscopic two-fluid equations for the superfluid and normal-fluid components are[7]

$$\rho_s \frac{d}{dt}\mathbf{V}_s = -\rho_s \nabla\mu - \mathbf{F} , \tag{1}$$

$$\rho_n \frac{d}{dt}\mathbf{V}_n = -\nabla(P-\rho_s\mu)+\eta\nabla^2\mathbf{V}_n+\mathbf{F} , \tag{2}$$

where the chemical potential μ and mutual friction $\mathbf{F}$ satisfy

$$\nabla\mu = -S\nabla T+\frac{1}{\rho}\nabla P-\frac{1}{2}\frac{\rho_n}{\rho}\nabla|\mathbf{V}_n-\mathbf{V}_s|^2 , \tag{3}$$

$$\mathbf{F}=\rho_s\kappa\times[n_+(\mathbf{V}_+-\mathbf{V}_s)-n_-(\mathbf{V}_--\mathbf{V}_s)] . \tag{4}$$

The positive and negative superfluid vortices have circulations $\pm\kappa=\pm(h/m)\hat{\mathbf{z}}$, densities $n_\pm$, and line velocities $\mathbf{V}_\pm$. The latter are related to $\mathbf{V}_s$ and $\mathbf{V}_n$ by

$$\mathbf{V}_\pm=\mathbf{V}_s+f'(\mathbf{V}_n-\mathbf{V}_s)\pm f\hat{\mathbf{z}}\times(\mathbf{V}_n-\mathbf{V}_s) . \tag{5}$$

The numerical values of f and f' used here are taken from second-sound attenuation measurements of the standard friction parameters B and B',[8,9]

$$f=\rho_n B/2\rho, \quad f'=\rho_n B'/2\rho \ . \tag{6}$$

The dissipation is sufficiently small in the counterflows considered here to neglect superfluid conversion and temperature variation.

Also needed are the conservation equations for the vortex densities,

$$\frac{\partial}{\partial t}n_\pm+\nabla\cdot n_\pm V_\pm=-\sigma n_+ n_- \ , \tag{7}$$

where the decay parameter σ is the cross section per unit time for mutual annihilation of antiparallel vortices. Equations (1) and (7) are not independent since

$$\nabla\times\mathbf{V}_s=n\boldsymbol{\kappa} \ , \tag{8}$$

where n is the net vortex density,

$$n=n_+-n_- \ . \tag{9}$$

It is easy to verify the consistency of these equations. Rewriting Eq. (1) as

$$\frac{\partial}{\partial t}\mathbf{V}_s+n_+\boldsymbol{\kappa}\times\mathbf{V}_+-n_-\boldsymbol{\kappa}\times\mathbf{V}_-=-\nabla(\mu/\rho_s+V_s^2/2) \ ,$$

and taking the curl gives the same conservation equation for n as does Eq. (7),

$$\frac{\partial}{\partial t}n+\nabla\cdot n[\mathbf{V}_s+f'(\mathbf{V}_n-\mathbf{V}_s)]+\nabla\cdot Nf\hat{\mathbf{z}}\times(\mathbf{V}_n-\mathbf{V}_s)=0 \ , \tag{10}$$

where N is the total vortex density,

$$N=n_++n_- \ . \tag{11}$$

N is the independent component of Eq. (7) and satisfies the conservation equation

$$\frac{\partial}{\partial t}N+\nabla\cdot N[\mathbf{V}_s+f'(\mathbf{V}_n-\mathbf{V}_s)]+\nabla\cdot nf\hat{\mathbf{z}}\times(\mathbf{V}_n-\mathbf{V}_s)=-\tfrac{1}{2}\sigma(N^2-n^2) \ . \tag{12}$$

By ignoring density fluctuations the decay parameter σ can be found to first order by calculating the decay time τ for isolated, opposite vortices a distance r apart,

$$\tau=\pi r^2/2f\kappa \ .$$

The average distance between a positive vortex and a given negative vortex is $r^2=1/\pi n_+$, and the decay of the negative vortices obeys

$$\dot{n}_-=-n_-/\tau \ .$$

Substituting for τ and r and comparing with Eq. (7) gives

$$\sigma=2\kappa f \ . \tag{13}$$

B. Radial counterflow and the steady-state N and n equations

In cylindrical coordinates r,ϕ the radial components of $\mathbf{V}_s$ and $\mathbf{V}_n$ are fixed by the counterflow condition

$$\rho_s V_{sr}+\rho_n V_{nr}=0 \ , \tag{14}$$

where $V_{nr}=W/r$, W being a constant. For convenience, W and its dimensionless form, $w=W/\Omega r_2^2$, will be called counterflow. It is assumed the flows are cylindrically symmetric, so the angular components of the velocities obey

$$\rho_s\frac{\partial}{\partial t}V_{s\phi}+\rho_s V_{sr}\frac{1}{r}\frac{\partial}{\partial r}rV_{s\phi}=-F_\phi \ , \tag{15}$$

$$\rho_n\frac{\partial}{\partial t}V_{n\phi}+\rho_n V_{nr}\frac{1}{r}\frac{\partial}{\partial r}rV_{n\phi}=F_\phi+\eta\frac{\partial}{\partial r}\frac{1}{r}\frac{\partial}{\partial r}rV_{n\phi} \ , \tag{16}$$

$$F_\phi=-\rho_s\kappa[Nf(V_{n\phi}-V_{s\phi})-nf'(V_{nr}-V_{sr})] \ . \tag{17}$$

The net vortex density n and the trapped circulation around the inner cylinder determine $V_{s\phi}$ in a simple manner, since the circular symmetry cancels the flow due to vortex images. Explicitly,

$$V_{s\phi}(r,t)=\frac{\kappa}{r}\left[\int_{r_1}^{r}r'dr'n-r_1\int_0^t dt'(n_+V_{+r}-n_-V_{-r})_{r_1}\right]+\frac{r_1}{r}V_{s\phi}(r_1,0) \ , \tag{18}$$

where r_1 is the radius of the inner cylinder. The integral over time in Eq. (18) accounts for the change in trapped circulation due to vortex flux at r_1.

A general solution requires the initial conditions $V_{s\phi}(r_1,0)$, $V_{n\phi}(r,0)$, $n_+(r,0)$, and $n_-(r,0)$, and the boundary conditions $n_\pm(r_1,t)$, $n_\pm(r_2,t)$, $V_{nr}(r_2,t)$, $V_{n\phi}(r_1,t)=\Omega r_1$, and $V_{n\phi}(r_2,t)=\Omega r_2$, where r_2 is the radius of the outer boundary. The boundary conditions on $n_\pm$ are needed only where the vortex velocity is directed into the fluid. Being dissipative, the system moves to a steady-state fixed point (for a sufficiently small driving force) which appears to be independent of the initial conditions. (Being nonlinear, the system should show a transition to chaos for increasing driving force.)

In the case of steady state it is possible to reduce Eqs. (10), (12), (15), and (16) to only two, for N and n. The derivation proceeds by assuming $N>0$ and noting that the vortex fluxes must cancel (in steady state) at all points,

$$n_+V_{+r}=n_-V_{-r} \tag{19}$$

where, from Eq. (5),

$$V_{\pm r}=-YW/r\mp f(V_{n\phi}-V_{s\phi}) \ . \tag{20}$$

Therefore, Eq. (19) becomes

$$YWn/r+f(V_{n\phi}-V_{s\phi})N=0 \ , \tag{21}$$

where

$$Y=(\rho_n-f'\rho)/\rho_s \ .$$

Substituting Eq. (21) successively in Eqs. (12) and (16) gives, respectively,

$$\frac{1}{r}\frac{\partial}{\partial r}N(1-x^2)-\left[\frac{\sigma}{2YW}\right]N^2(1-x^2)=0 \ , \tag{22}$$

$$r\frac{\partial^2}{\partial r^2}x-\left[1+\frac{W\rho_n}{\eta}\right]\frac{\partial}{\partial r}x-\left[\frac{\kappa f}{YW}\right]r^2\frac{\partial}{dr}Nx=0 \ , \tag{23}$$

where $x=n/N$. If these nonlinear equations could be solved for N and n, then $V_{s\phi}$ would follow at once from Eq. (18) and $V_{n\phi}$ from Eq. (21). Over intervals where $N=0$, Eq. (16) can be solved exactly for $V_{n\phi}$.

C. Exact solutions (restricted vortex nucleation)

There is a one-parameter family of simple, exact solutions of Eqs. (22) and (23) for the case that n_- is everywhere zero. This means $N=n$, so Eq. (23) requires that N be constant, i.e., n_+ itself is constant. (The asymmetry between n_+ and n_- is a result of assuming that the angular velocity Ω of the container is positive.)

The family is parametrized conveniently by the amount of vorticity within r_2 when the counterflow $V_{nr}=W/r$ is positive, and by the circulation around r_1 when the counterflow is negative. Specifically, the solutions can be labeled by a parameter α, defined by

$$\alpha=\begin{cases} V_{s\phi}(r_2)/\Omega r_2, & W>0 \\ V_{s\phi}(r_1)/\Omega r_1, & W<0 \end{cases}.$$

For fixed counterflow W there is only one value of α that corresponds to constant vorticity filling the region between r_1 and r_2. This particularly simple solution is called solid-body rotation (SBR) because of its similarity to equilibrium. The SBR solution occurs if only positive vortices are allowed to enter the liquid when counterflow is applied to rotational equilibrium. This is also a limiting solution in the sense that there are no solutions of larger (smaller) α for positive (negative) W.

For other values of α the constant vorticity is interrupted by a vortex-free gap at one of the boundaries. This is called the conserved-vorticity (CV) solution because it occurs if no additional vortices enter the liquid when counterflow is imposed on rotational equilibrium. These two solutions will now be given in detail.

1. *Nucleation of positive vortices (solid-body rotation, SBR)*

This solution is easily found from Eq. (21). Setting $n=N$ and evaluating at r_1 gives

$$V_{s\phi}(r_1)=\Omega r_1+(YW/f)/r_1 \ . \tag{24}$$

Using this in Eq. (18),

$$v_{s\phi}=\frac{n_+\kappa}{r}\tfrac{1}{2}(r^2-r_1^2)+\frac{r_1}{r}\left[\Omega r_1+\frac{YW}{f}\frac{1}{r_1}\right],$$

and comparing with Eq. (21) evaluated at r_2 gives

$$n_+=2\Omega/\kappa, \quad r_1\le r\le r_2 \ . \tag{25}$$

This is the same vortex density that occurs in equilibrium. The only effect of counterflow is to change the magnitude of trapped circulation around the inner cylinder; for $W<0$ this circulation can even be negative, according to Eq. (24). It is convenient to represent the trapped circulation by an equivalent vortex density n_e inside r_1,

$$n_e=2V_{s\phi}(r_1)/\kappa r_1 \ .$$

Finally, $V_{n\phi}$ can be found from Eq. (21), by substituting the above expressions for $V_{s\phi}$ and n_+,

$$V_{n\phi}=\Omega r \ , \tag{26}$$

i.e., solid-body rotation. The parameter $\alpha_{\rm SBR}$ for this solution is

$$\alpha_{\rm SBR}=\begin{cases} 1+YW/(f\Omega r_2^2), & W>0 \\ 1+YW/(f\Omega r_1^2), & W<0 \ . \end{cases} \tag{27}$$

Whether or not this is also the physical solution (apart from presumably small and controllable three-dimensional effects) depends on the unknown boundary condition for negative vortices in a positively rotating container. From Eq. (20) it is obviously impossible to have zero vortex velocity at the boundaries simultaneously for both vortex species whenever the counterflow is finite. *So, the SBR solution is physically unstable to the entrance of negative vortices from the boundary,* either outer or inner as W is positive or negative. Within the two-fluid model there is no basis to rule out the entrance of negative vortices.

Figures 1 and 2 show the angular velocities $V_{n\phi}, V_{+\phi}$ and vortex densities for $W/\Omega r_2^2=\pm 0.1$. The difference between $V_{n\phi}$ and $V_{+\phi}$ remains fairly constant between r_1 and r_2, and changes sign according to the direction of counterflow W. The equivalent vortex density n_e inside r_1 is also strongly affected by the sign of W.

The values of the superfluid parameters[9] used here and elsewhere in the paper correspond to ^{4}He at $T=1.7$ K, viz., $\eta/\rho_n=3.17\times 10^{-4}$ cm^2/sec, $f=0.127$, $f'=0.0122$, and $\rho_s/\rho=0.768$.

2. *No vortex nucleation (conserved vorticity, CV)*

These solutions correspond to finite regions of vorticity which do not fill the entire volume when α is between

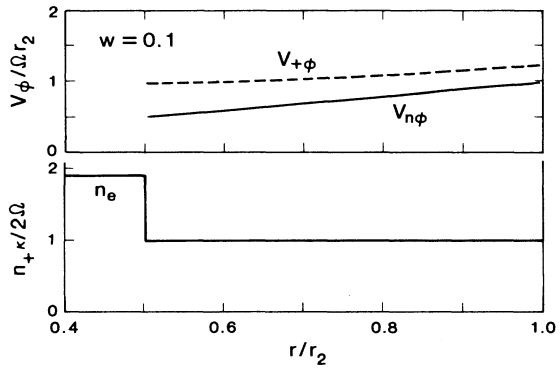

FIG. 1. Upper: Angular velocities of normal fluid (solid curve) and positive vortices (dashed curve) as a function of radial position in the annulus. Nucleation at the boundary of positive (negative) vortices is unrestricted (suppressed), resulting in a vortex density distribution and an angular component of normal fluid velocity equal to solid-body rotation (SBR). Lower: Accompanying vortex density distribution. The macroscopic superfluid circulation around the inner boundary r_1 is denoted by an equivalent, but fictitious, vortex density n_e in the region $r<r_1=0.5r_2$. The counterflow parameter $w=0.1$ (inner boundary hotter than outer boundary).

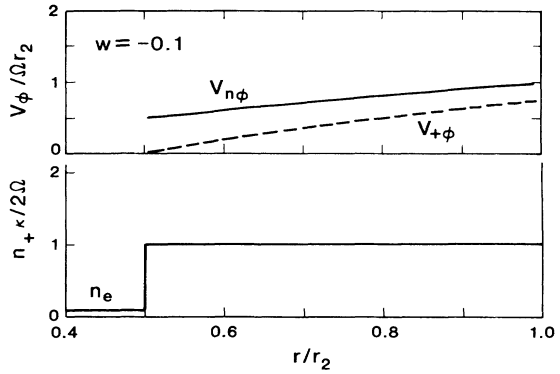

FIG. 2. Same as Fig. 1 for opposite counterflow (inner boundary colder).

the limits

$$\alpha_{\rm SBR}-1+(r_1/r_2)^2<\alpha<\alpha_{\rm SBR},\quad W>0$$
$$\alpha_{\rm SBR}<\alpha<\alpha_{\rm SBR}-1+(r_2/r_1)^2,\quad W<0\ . \tag{28}$$

The case $\alpha\neq 1$ corresponds to both counterflow *and* a change in rotational velocity being imposed on superfluid in equilibrium rotation, with no additional vortices entering. In the region where $n_+>0$ the solution is found as before from Eq. (21). However, a gap of zero vorticity now occurs at the cold boundary, i.e., at the outer or inner boundary for W greater or less than zero, respectively. In this gap Eq. (16) is easily solved for $V_{n\phi}$ because $F_\phi=0$. Then the solutions for $V_{s\phi}$ and $V_{n\phi}$ are joined at the boundary r_3 between the vortex-filled and vortex-free regions by making $V_{s\phi}$, $V_{n\phi}$, and $\partial V_{n\phi}/\partial r$ continuous. This gives an equation for r_3 which can be solved numerically. The general solution is given in Table I.

Typical behavior of the gap position r_3 and the vortex density n_+ as a function of W is shown in Fig. 3 for $\alpha=1$. The gap expands and then contracts somewhat as the counterflow $|W|$ increases while the vortex density decreases monotonically, reaching zero when the limit (opposite $\alpha_{\rm SBR}$) is approached in Eq. (28). Angular velocities and vortex densities for $W/\Omega r_2^2=\pm 0.1$ are shown in Figs. 4 and 5.

Like the SBR solution the CV solution is also physically (not mathematically) unstable, in this case *unstable*

TABLE I. Exact solution of the two-fluid dissipative equations describing radial counterflow in a positively rotating annulus of inner (outer) radius r_1 (r_2) when the negative vortex density is everywhere zero. The parameter W gives the strength of the radial counterflow velocity, $W=rV_{nr}$. The radius r_3 is the boundary of the vortex region and is defined by $h_3=0$. The square brackets $[r_1,r_3]$, etc. under r define the region of the given solution for the vortex density $n_+\kappa/2\Omega$ and the normal-fluid angular velocity $v_{n\phi}/\Omega r_2$. The various functions h_0, etc. are defined in the lower part of the table along with the independent parameters α and A. The special case $A=-2$ requires the solution given at the bottom of the table. Also, $Y\equiv(\rho_n-f'\rho)/\rho_s$.

W	r_3	r	$\frac{n_+\kappa}{2\Omega}\equiv c$	$V_{n\phi}/\Omega r_2$
>0	$h_3(r_1,r_2,r_3)=0$	$[r_1,r_3]$	$h_2(r_1,r_2)$	$\frac{r_1^2(1-c)}{r_2}\frac{1}{r}+\frac{c}{r_2}r$
		$[r_3,r_2]$	0	$h_1(r_1)\frac{1}{r_2 r}+h_0 r^{1+A}$
<0	$h_3(r_2,r_1,r_3)=0$	$[r_1,r_3]$	0	$h_1(r_2)\frac{1}{r_2 r}+h_0 r^{1+A}$
		$[r_3,r_2]$	$h_2(r_2,r_1)$	$(1-c)r_2\frac{1}{r}+\frac{c}{r_2}r$

$$h_0=\frac{2c}{(2+A)r_2 r_3^A},\quad A=\frac{W\rho_n}{\eta},\quad \alpha=\begin{cases}V_{s\phi}(r_2)/\Omega r_2, & W>0\\ V_{s\phi}(r_1)/\Omega r_1, & W<0\end{cases}$$

$$h_1(r_1)=r_1^2+c\left[\frac{Ar_3^2}{2+A}-r_1^2\right]$$

$$h_2(r_1,r_2)=(\alpha r_2^2-r_1^2-YW/\Omega f)/(r_3^2-r_1^2)$$

$$h_3(r_1,r_2,r_3)=h_2(r_1,r_2)[2(r_2^{2+A}-r_1^2 r_3^A)+A(r_3^2-r_1^2)r_3^A]-(2+A)(r_2^2-r_1^2)r_3^A=0$$

Special case $A=-2$

$$2r_3^2(r_2^2-\alpha r_1^2+YW/\Omega f)\ln(r_3/r_1)+[(1-\alpha)r_1^2+YW/\Omega f](r_2^2-r_3^2)=0\quad\text{determines } r_3$$

$$\frac{V_{n\phi}}{\Omega r_2}=\frac{r_2^2+c(r_3^2-r_2^2)}{rr_2}+\frac{cr_3^2\ln(r/r_3)}{r_1 r_2},\quad r_1\le r\le r_3$$

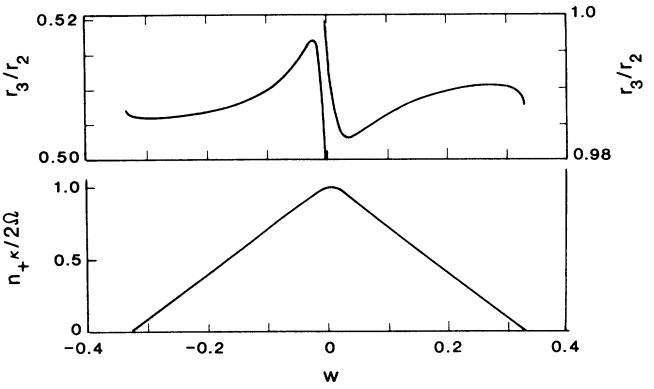

FIG. 3. Upper: The position of the boundary r_3 that separates vortex-free and vortex-filled regions of the annulus when all vortex nucleation is suppressed (conserved vorticity, CV) as a function of counterflow w. The left- (right-) hand scale is associated with negative (positive) w. Lower: Vortex density for the CV solution in the upper graph. The vortex density loses its symmetry around $w=0$ when $\alpha\neq 1$ (see text for definition of α).

to the entry of both positive and negative vortices. For $\alpha=1$ the two vortex velocities into the fluid at the physical boundary of the gap are equal.

(The existence of a gap at the outer boundary r_2 for counterflow $W>0$ is a favorable condition for the propagation of generalized Kelvin waves on the boundary r_3 of the vortex region.[10,11] The previous derivation of these waves[11] can be repeated for the case of radial counterflow, and gives the complex dispersion relation

$$\frac{\omega}{m}=\frac{1}{r_3}V_{+\phi}-(1-f'+if)\frac{\Omega}{m}\left[1-\left[\frac{r_3}{r_2}\right]^{2m}\right], \tag{29}$$

where ω is the frequency and m the number of maxima of the circular wave. Only the first term on the right-hand side of Eq. (29) differs from the result of Ref. 11, and has the interpretation of being the wave velocity when $m\to\infty$, which must be the velocity of the outermost ring of vortices.)

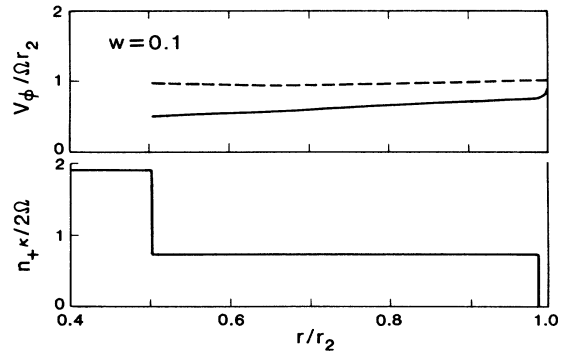

FIG. 4. Same as Fig. 1 for the case that all vortex nucleation is suppressed (CV).

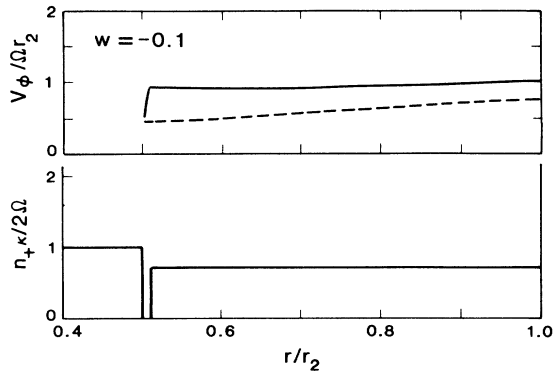

FIG. 5. Same as Fig. 4 for opposite counterflow.

D. Numerical solutions (unrestricted vortex nucleation)

For the case that both positive and negative vortices are nucleated at the boundary no exact solutions are known. In principle, one could numerically solve the N and n equations, Eqs. (22) and (23), but it is more instructive to integrate the original dynamical equations over time until a fixed point is reached. A convenient choice of independent equations consists of those for the normal fluid velocity $V_{n\phi}$ and the two vortex densities $n_\pm$ [Eqs. (16) and (7)] with the boundary conditions $V_{n\phi}(r_b,t)=\Omega r_b$, $n_\pm(r_b,t)=n_\pm^0>0$, where $r_b=r_1,r_2$. The superfluid velocity $V_{s\phi}$ is then determined by Eq. (18).

The equations were solved by a finite-difference method on a staggered mesh (alternating densities and velocities) using standard donor-cell differencing and iteration of implicit solutions of the finite-difference equations. Various consistency checks were performed to verify the correctness of the solutions. These included reproduction of the exact solutions, independence of the final solution with respect to initial conditions, invariance with expansion of scale, and agreement between different solution methods. About 200 spatial grid points are sufficient to resolve the behavior, except near the cold boundary, where $\partial V_{n\phi}/\partial r$ is large and a finer mesh is needed. For the cases shown here about 2000 time steps are sufficient to reach steady state; the exact number depends on the initial conditions, the criterion for steady state, and how conservatively the size of the time steps is chosen for numerical stability.

Figures 6 and 7 show angular velocities and vortex densities for the same counterflows $W/\Omega r_2^2=\pm 0.1$ and temperature $T=1.7$ K as before. The small plus sign on the right-hand side of the vortex density graphs shows the average of $n\kappa/2\Omega$ between the boundaries, and the small horizontal line extends the average to include n_e, i.e., its value is $V_{s\phi}(r_2)/\Omega r_2$. The positive and negative vortex densities at the boundary are given the same value,

$$n_\pm^0\kappa/2\Omega=1\ .$$

The most obvious change from the previous solutions is the large maximum in positive vortex density n_+ near the cold boundary, resulting in a sort of "space charge"

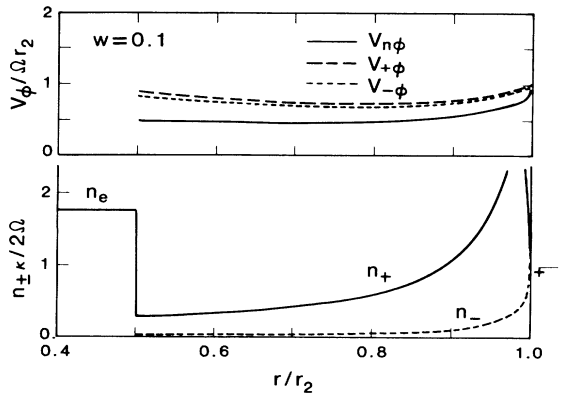

FIG. 6. Same as Fig. 1 for the case of unrestricted vortex nucleation (UVN).

of vorticity. The maximum is itself approximately maximum at the counterflow value used here.

The negative vortex density n_- decreases monotonically from the cold to the hot boundary. Unlike the previous solutions there is a steady flux of total vorticity from the cold to hot boundary. Because positive and negative vortices mutually annihilate, the magnitude of this flux decays over distance, but the vortex densities at any location are constant in time.

Both vortex angular velocities $V_{\pm\phi}$ either lead or lag behind the normal velocity $V_{n\phi}$ for positive or negative counterflow, respectively. The greatest lead or lag always occurs for $V_{+\phi}$. It is this relative velocity $V_{\pm\phi}-V_{n\phi}$ that causes most of the dissipation in the interior of the fluid.

Equating the vortex fluxes at the cold boundary $n_+^0 V_{+r}=n_-^0 V_{-r}$ gives

$$\frac{n_-^0}{n_+^0}=\frac{-YW/r_b-f[\Omega r_b-V_{s\phi}(r_b)]}{-YW/r_b+f[\Omega r_b-V_{s\phi}(r_b)]} .$$

Therefore, $n_+^0=n_-^0$ implies $V_{s\phi}(r_b)=\Omega r_b$. This is the equilibrium superfluid velocity in the absence of counterflow, so no net vorticity leaves the cold boundary during the approach to steady state (starting from an equilibrium state without counterflow). (The values of $n_\pm^0$ are irrelevant at the hot boundary because it is never a source in steady state.) The qualitative nature of the solution is not sensitive to the exact, finite values of $n_\pm^0$. Reducing $n_\pm^0$ by a factor of 10 reduces the maximum of $n_+(r)$ by a factor of 2 or less, and changes the meniscus profile by roughly 10%. Of course, the solution is quite sensitive to zero values of $n_\pm^0$, and for $n_\pm^0\to 0$ the solution slowly approaches the corresponding exact solutions for restricted vortex nucleation.

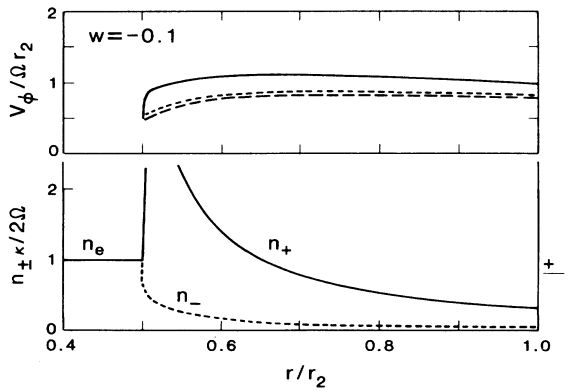

FIG. 7. Same as Fig. 6 for opposite counterflow.

Because the dynamical equations are used to find the steady-state solutions, information on the transient behavior is obtained, as well. For example, starting from rotational equilibrium without counterflow, the steady state in Figs. 6 and 7 is reached in about $70/\Omega$ s after the counterflow is switched on. The maximum in the vortex density establishes itself sooner, in about $40/\Omega$ s. Doubling the counterflow velocity reduces the time to reach steady state to about $10/\Omega$ s.

III. PROPERTIES

A. Dissipation

Multiplying Eqs. (1) and (2) by $\mathbf{V}_s$ and $\mathbf{V}_n$, respectively, adding, and integrating over the volume gives an equation for the time rate of change of the kinetic energy, which is the dissipation rate. In steady state this energy loss is sustained by forces at the boundaries, such as a temperature difference in the case of counterflow. The dissipation consists of two parts.

1. Viscous dissipation

This occurs only for the normal fluid, and has the well-known form[12]

$$D_\eta=-\tfrac{1}{2}\eta\int d^2r(\sigma'^2_{rr}+2\sigma'^2_{r\phi}+\sigma'^2_{\phi\phi}) , \tag{30}$$

where

$$\sigma'_{rr}=2\frac{\partial V_{nr}}{\partial r} ,$$

$$\sigma'_{r\phi}=\frac{1}{r}\frac{\partial V_{nr}}{\partial\phi}+\frac{\partial V_{n\phi}}{\partial r}-\frac{V_{n\phi}}{r} ,$$

$$\sigma'_{\phi\phi}=2\left[\frac{1}{r}\frac{\partial V_{n\phi}}{\partial\phi}+\frac{V_{nr}}{r}\right] .$$

It will be convenient to express the results as a dimensionless viscous dissipation density d_η, defined as

$$D_\eta=-\rho\Omega^3 r_2^2\int d_\eta d^2r . \tag{31}$$

For the case here of angular symmetry and counterflow,

$$d_\eta=\frac{\eta}{\rho\Omega r_2^2}\left[4\left[\frac{W}{\Omega r_2^2}\right]^2\left[\frac{r_2}{r}\right]^4+\left[\frac{\partial V_{n\phi}}{\partial r}-\frac{V_{n\phi}}{r}\right]^2\frac{1}{\Omega^2}\right] . \tag{32}$$

2. Vortex dissipation

This takes the form

$$D_v = -\rho_s \kappa f \int d^2 r\, N \mid \mathbf{V}_s - \mathbf{V}_n \mid^2 , \tag{33}$$

or, in terms of a dimensionless vortex dissipation density d_v, defined like d_η in Eq. (31),

$$d_v = 2\frac{\rho_s}{\rho} fN \left[\left[\frac{\rho}{\rho_s} \right]^2 \left[\frac{W}{\Omega r_2^2} \right]^2 \left[\frac{r_2}{r} \right]^2 + (V_{s\phi} - V_{n\phi})^2 \frac{1}{(\Omega r_2)^2} \right] . \tag{34}$$

The total dissipation is sustained by the temperature difference across the two boundaries,

$$2\pi\rho S r V_{nr} T \mid_{r_1}^{r_2} = D_\eta + D_v ,$$

or

$$T_2 - T_1 = \frac{D_\eta + D_v}{2\pi\rho S W} . \tag{35}$$

The temperature differences of interest are so small that the entropy S can be taken as constant over the volume.

B. Meniscus

One of the ways the vortex distribution can reveal itself is through the shape of the meniscus at the free surface. Capillarity and surface tension will be ignored, because the capillary constant for helium is only of order 0.07 cm and the curvature of the miniscus is small.

To find the meniscus, add the radial components of Eqs. (1) and (2) to obtain an expression for $\partial P/\partial r$ and integrate from r_1 to r. The change in height Δz is related to ΔP by ρ and the gravitational constant g,

$$\Delta z(r) = \frac{\Delta P}{\rho g} = \frac{1}{g} \left[-\frac{1}{2}\frac{\rho_n}{\rho_s} V_{nr}^2 \Big|_{r_1}^{r} + \int_{r_1}^{r} \frac{dr'}{r'} \left[\frac{\rho_s}{\rho} V_{s\phi}^2 + \frac{\rho_n}{\rho} V_{n\phi}^2 \right] \right] . \tag{36}$$

In Figs. 8 and 9 are shown different menisci corresponding to no counterflow, and to positive and negative counterflow using the SBR, CV ($\alpha = 1$), and unrestricted vortex nucleation (UVN) solutions given earlier. Clearly, the meniscus can distinguish different vortex nucleation boundary conditions.

C. Heat torque and angular momentum

The torque induced by radial counterflow on a stationary boundary with trapped circulation was considered by Penney and Overhauser.[13] The more general results for a rotating container are quite different. The torque τ on the liquid is the time derivative of the total angular momentum, so multiplying Eqs. (15) and (16) by r, adding, and integrating over the volume gives

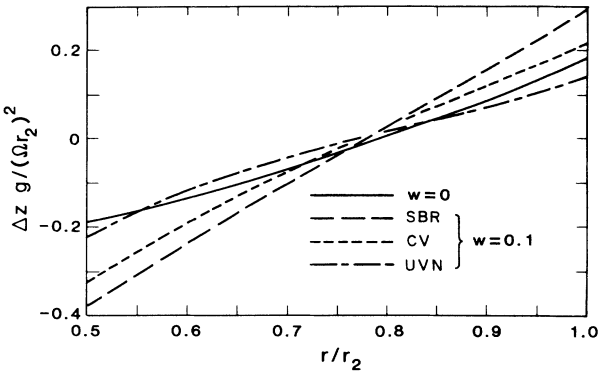

FIG. 8. Meniscus profiles corresponding to the solutions in Figs. 1, 4, and 6.

$$\tau = \frac{\partial}{\partial t} 2\pi \int_{r_1}^{r_2} dr\, r^2 (\rho_s V_{s\phi} + \rho_n V_{n\phi}) = 2\pi r^2 \left[\rho_n V_{nr} (V_{s\phi} - V_{n\phi}) + \eta \left[\frac{\partial V_{n\phi}}{\partial r} - \frac{v_{n\phi}}{r} \right] \right] \Bigg|_{r_1}^{r_2} , \tag{37}$$

after making use of the conservation equations for ρ_s and ρ_n, and of the counterflow condition, Eq. (14).

According to Eq. (37) the torque τ_1 (per unit length) on the inner cylinder is

$$\tau_1 = 2\pi r_1^2 \left[\rho_n V_{nr} (V_{s\phi} - V_{n\phi}) + \eta \left[\frac{\partial V_{n\phi}}{\partial r} - \frac{V_{n\phi}}{r} \right] \right]_{r_1} . \tag{38}$$

In the absence of rotation, $V_{n\phi} = 0$, and Eq. (38) reduces to the result of Ref. 13,

$$\tau_1 = \mathcal{N} Q / m S_n T, \quad \Omega = 0 ,$$

where $\mathcal{N}$ is the number of circulation quanta trapped around r_1, Q is the counterflow heat flux per unit length ($Q = 2\pi r \rho S T V_{nr}$), m is the ^{4}He mass, and $S_n = \rho S/\rho_n$.

In the presence of rotation, the torque τ changes qualitatively. For example, the SBR solution has $V_{n\phi} = \Omega r$

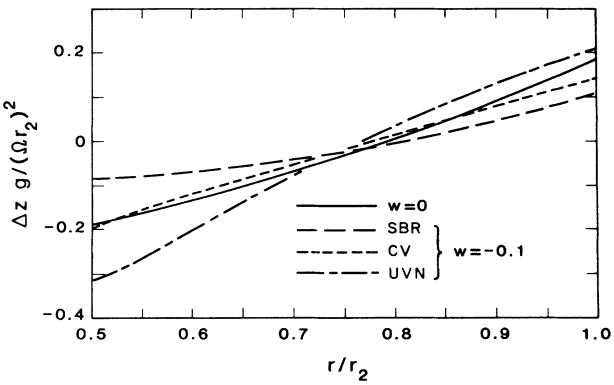

FIG. 9. Meniscus profiles corresponding to the solutions in Figs. 2, 5, and 7.

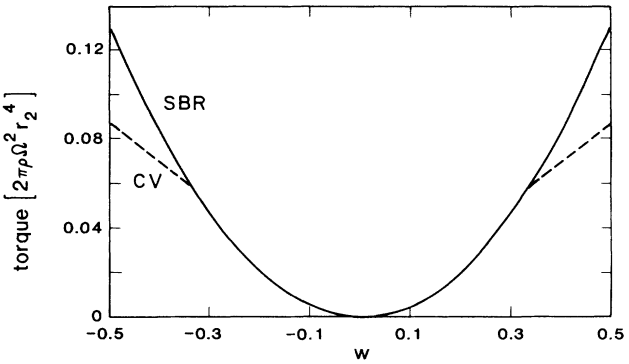

FIG. 10. Torque per unit length on inner cylinder as a function of counterflow for the SBR and CV solutions.

and

$$V_{s\phi}=\Omega r+\frac{YW}{f}\frac{1}{r} ,$$

so

$$\tau_1=2\pi\rho_n(Y/f)W^2=YQ^2/(2\pi\rho_n f S_n^2 T^2) , \tag{39}$$

i.e., the torque is *quadratic* in Q. The torque on the outer boundary is equal and opposite, so the container experiences shear stress of the same sign, independent of the direction of heat flow. Figure 10 shows the torque on the inner boundary as a function of counterflow for both the SBR and CV ($\alpha=1$) solutions. The change in behavior of the CV solution occurs at the point where vorticity in the fluid disappears, $|W|=(\Omega f/Y)(r_2^2-r_1^2)$, for $\alpha=1$. The overlap of the curves in the quadratic region is not exact.

The steady-state angular momentum of the fluid can differ substantially from the equilibrium angular momentum (i.e., for the same rotation but not counterflow), so the transient heat torques on the container at r_1 and r_2 are certainly unequal. Explicitly, the angular momentum (per unit length) is

$$L=2\pi\int_{r_1}^{r_2} r^2 dr(\rho_n V_{n\phi}+\rho_s V_{s\phi}) , \tag{40}$$

which becomes

$$L_0=\pi\rho\Omega(r_2^4-r_1^4)/2 \tag{41}$$

for no counterflow. The SBR solution has angular momentum

$$L_{\rm SBR}=L_0+\pi\rho_s YW(r_2^2-r_1^2)/f . \tag{42}$$

The CV angular momentum is always less than that for SBR (because the vorticity is less). The expression for $L_{\rm CV}$ is not particularly illuminating and will not be shown, but $L_{\rm CV}$ and $L_{\rm SBR}$ are compared in Fig. 11 for the same example used in Fig. 10. Even though the steady-state shear stress on the container is essentially the same for the two solutions over a wide range of counterflow velocity, the angular momentum is not, so counterflow applied to a freely rotating container would distinguish between CV and SBR solutions by the steady-state rotation rate.

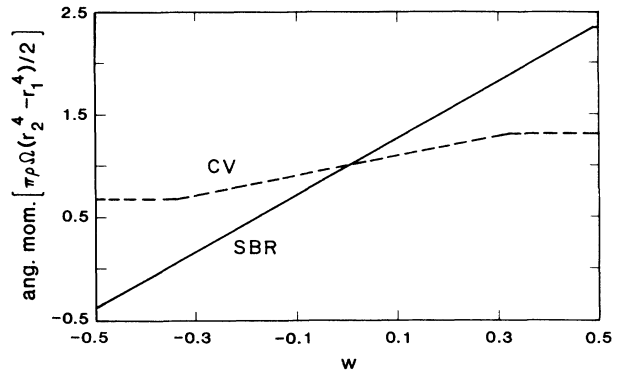

FIG. 11. Angular momentum per unit length of the liquid as a function of counterflow for the SBR and CV solutions.

IV. SUMMARY

The phenomenological two-fluid superfluid equations of Landau have the deficiency that they cannot be used to calculate common superfluid phenomena, namely those involving superfluid vorticity. The conventional generalization of these equations to include the net vorticity $\nabla\times\mathbf{V}_s$ is sufficient for phenomena involving either parallel vortices of the same sign or regions so small that the motion of only single vortices is of concern (in which case the equations become quasimicroscopic and require spatial averaging to regain their direct predictive power for large-scale flow). The necessity to go beyond net vorticity and add total vorticity to the two-fluid equations is illustrated here in a simple two-dimensional example of driven, dissipative, steady-state flow. This example also demonstrates the importance of vortex flux boundary conditions (nucleation rates) in nonequilibrium flows. These boundary conditions are not calculable within the two-fluid model, and remain to be determined from a more microscopic theory or from experiments, which could be guided by these results.

The system here has the same geometry as Couette flow but, instead of imposing a difference in angular velocity by different rotation rates of the two boundaries at constant temperature, a radial counterflow velocity is imposed by a temperature difference across the boundaries at constant rotation. Starting from rotational equilibrium and applying the counterflow causes, variously, a gap or no change or a sharp maximum to appear in the positive vortex density at the cold boundary depending, respectively, on whether no vortices or only positive vortices or both positive and negative vortices are nucleated there. The simultaneous presence of both positive and negative vortices is possible, in principle, because the fluid dynamic forces favor the entrance of

both types into the liquid, where they mutually annihilate over some distance. Consequently, the steady-state vortex fluxes are nonzero if nucleation is unrestricted.

The results here assume angular symmetry. Based on the generic behavior of driven, dissipative systems this symmetry should break at some sufficiently high counterflow velocity which remains to be predicted, even in the linear approximation.

[1]E. L. Andronikashvili and Yu. G. Mamaladze, Rev. Mod. Phys. **38**, 567 (1966).

[2]A. L. Fetter, Phys. Rev. **153**, 285 (1967).

[3]I. M. Khalatnikov, *An Introduction to the Theory of Superfluidity* (Benjamin, New York, 1965), Chap. 16.

[4]R. J. Donnelly and C. E. Swanson, J. Fluid Mech. **173**, 387 (1986).

[5]L. J. Campbell and Yu. K. Krasnov, J. Low Temp. Phys. **49**, 377 (1982).

[6]P. W. Adams, M. Cieplak, and W. I. Glaberson, Phys. Rev. B **32**, 171 (1985).

[7]J. Wilks, *The Properties of Liquid and Solid Helium* (Clarendon, Oxford, 1967), Chap. 13.

[8]P. Lucas, J. Phys. C **3**, 1180 (1970).

[9]C. F. Barenghi, R. J. Donnelly, and W. F. Vinen, J. Low Temp. Phys. **52**, 189 (1983).

[10]E. B. Sonin, Rev. Mod. Phys. **59**, 87 (1987).

[11]L. J. Campbell and Yu. K. Krasnov, Phys. Lett. **84A**, 75 (1981). The Kelvin-type waves represented by Eq. (29) are generalized in three ways: for dissipation, for a finite container, and for radial flow.

[12]L. D. Landau and E. M. Lifshitz, *Fluid Mechanics* (Pergamon, London, 1959), Sec. 15.

[13]R. Penney and A. W. Overhauser, Phys. Rev. **164**, 268 (1967).